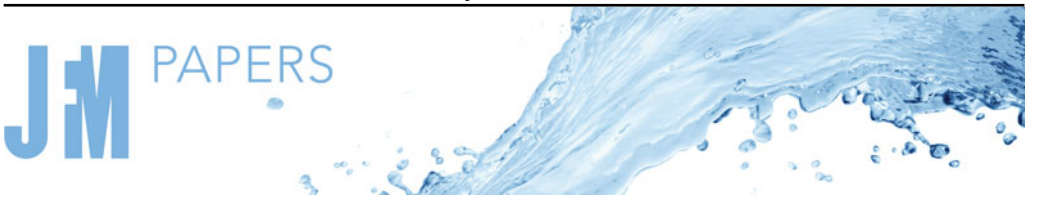
J. Fluid Mech. (2026), *vol.* 1037, A55, doi:10.1017/jfm.2026.11735



On acoustic–gravity wave triad resonance over an elastic half-space

Usama Kadri

School of Mathematics, Cardiff University, Cardiff, UK

Corresponding author: Usama Kadri, kadriu@cardiff.ac.uk

(Received 6 February 2026 UTC; revised 23 April 2026 UTC; accepted 29 May 2026 UTC)

Nonlinear interactions between free-surface gravity waves and acoustic–gravity motions provide a mechanism for energy exchange in weakly compressible fluids and have long been discussed in connection with microseisms and low-frequency underwater sound. While elastic solid-Earth response has been incorporated in microseism modelling, existing formulations of acoustic–gravity wave resonant triads are almost exclusively developed for a rigid seabed, which introduces a shallow-water cutoff where the acoustic–gravity member becomes evanescent and resonance cannot occur. Here, we extend the resonant-triad framework to a compressible fluid over an elastic half-space. Seabed elasticity modifies the acoustic–gravity eigenstructure and dispersion relation, admitting propagating or interface-guided acoustic–gravity modes in regimes inaccessible under rigid-bottom assumptions and thereby removing the rigid cutoff in frequency (or depth). Using a multiple-scale expansion in the small compressibility parameter, we derive modulation equations for two counter-propagating gravity waves coupled to a single elastic acoustic–gravity mode. A key feature is an interfacial term in the solvability condition arising from the parameter dependence of the elastic boundary operator, which alters the modal normalisation and the resulting coupling and detuning coefficients. The enlarged admissible parameter space also makes laboratory-scale realisations of acoustic–gravity triad resonance substantially more feasible, enabling controlled investigation of the triad mechanism.

Key words: acoustics, elastic waves, nonlinear dynamical systems

1. Introduction

Compressibility is commonly neglected in surface gravity-wave theory because acoustic and gravity waves typically propagate on widely separated temporal and/or spatial scales. In the linear regime, this separation justifies treating surface gravity waves as effectively decoupled from compressional motions in the fluid interior. Nevertheless, weak

© The Author(s), 2026. Published by Cambridge University Press. This is an Open Access article, distributed under the terms of the Creative Commons Attribution licence (https://creativecommons.org/licenses/by/4.0/), which permits unrestricted re-use, distribution and reproduction, provided the original article is properly cited.

https://doi.org/10.1017/jfm.2026.11735 Published online by Cambridge University Press

nonlinearity can couple these motions, allowing surface gravity waves to transfer energy into interior acoustic–gravity modes. This mechanism has long been implicated in geophysical and hydroacoustic phenomena, most notably microseisms and low-frequency sound in the ocean. In particular, solid-Earth (elastic) response has been included in microseism generation models in both classical and modern settings (Hasselmann 1963; Ardhuin & Herbers 2013). The present contribution is to incorporate elastic coupling into the weakly nonlinear acoustic–gravity resonant-triad framework and to identify the resulting interface term in the solvability condition and its implications for admissibility and coefficients. For brevity we occasionally refer to the triad's compressional member as the acoustic mode; throughout, this denotes the finite-depth acoustic–gravity eigenmode of the coupled system (acoustic in the bulk, gravity coupled through the free surface).

The possibility of compressibility-driven coupling between gravity and compressional motions was articulated in seminal work by Longuet-Higgins (1950), who showed that quadratic interactions of surface gravity waves can resonantly excite compressional modes in water of finite depth. In this framework, a pair of counter-propagating surface waves generates a depth-uniform pressure oscillation that couples efficiently to an interior acoustic–gravity mode when appropriate frequency-matching conditions are met. This established compressibility as a potentially important ingredient in nonlinear surface-wave dynamics, despite its negligible role at the linear level.

Subsequent studies clarified the structure and dispersion properties of acoustic–gravity waves and placed the compressibility-driven mechanism within the broader context of nonlinear wave interactions. In particular, pure surface gravity waves cannot form exact resonant triads among themselves (Phillips 1960), whereas coupling to acoustic–gravity modes permits resonant or near-resonant three-wave interactions. The general theory of resonant wave interactions developed by Bretherton (1964), and later synthesised by Phillips (1981) and Craik (1985), provides the natural framework for analysing such processes; see also Andrade *et al.* (2025) for a recent phase-space perspective.

A systematic treatment of acoustic–gravity interactions within this framework was developed by Kadri & Stiassnie (2013), and later refined by Kadri & Akylas (2016), who recast the compressibility-driven mechanism explicitly in terms of resonant (or weakly detuned) wave triads. In this setting, two nearly monochromatic gravity wavetrains interact to excite a nearly monochromatic acoustic–gravity wavetrain, and the slow exchange of wave action is governed by a closed set of modulation equations obtained by a weakly nonlinear multiple-scale expansion. This 'triad' description is a standard narrowband reduction valid on the slow modulation time scale selected by weak nonlinearity and weak compressibility; it does not assert global spectral confinement for arbitrary times, but rather captures the leading-order dynamics of the resonant components within the stated asymptotic ordering (Bretherton 1964; Craik 1985).

A central assumption underlying existing acoustic–gravity resonant-triad frameworks is that of a rigid seabed. While this simplifies the acoustic–gravity eigenproblem through a no-penetration boundary condition, it also imposes a significant physical limitation: in shallow water the acoustic–gravity member of the triad may become evanescent or be cut off entirely, precluding resonance and severely restricting the range of depths and frequencies for which the theory applies. As a result, laboratory-scale observation of acoustic–gravity triad resonance under rigid-bottom conditions is frequently impractical. On the other hand, fluid–solid coupling over elastic substrates is known to modify acoustic–gravity propagation in a fundamental way, supporting interface-guided or leaky modes and altering dispersion relations (Biot 1952; Achenbach 1973; Eyov *et al.* 2013). These effects have not yet been incorporated into the weakly nonlinear triad-resonance theory.

https://doi.org/10.1017/jfm.2026.11735 Published online by Cambridge University Press

The purpose of the present paper is to develop a theory of acoustic–gravity wave triad resonance for a weakly compressible fluid over an elastic half-space. The novelty is not the general observation that elasticity affects propagation, but the identification of how elastic coupling enters the triad reduction at a structural level: elasticity modifies the linear acoustic–gravity eigenproblem and, because the elastic boundary operator depends explicitly on the spectral parameters, it contributes an additional interfacial term to the solvability condition. This term modifies the acoustic–gravity mode normalisation and thus the coupling and detuning coefficients governing the triad dynamics. Importantly, elastic coupling can remove the rigid-bottom cutoff in frequency (or depth) by admitting propagating or interface-guided acoustic–gravity modes in regimes where the rigid problem supports only evanescence, thereby enlarging the admissible triad parameter space and making laboratory-scale realisations substantially more feasible.

2. Preliminaries

We consider two-dimensional irrotational motion of a weakly compressible, inviscid fluid of mean depth h over an elastic half-space. The undisturbed free surface is located at $z = 0$, the fluid resides in the region $-h \leqslant z \leqslant 0$ and the elastic solid occupies $z \leqslant -h$. Gravity acts in the negative z-direction.

2.1. *Fluid equations*

The fluid velocity is described by a velocity potential $\phi_l(x, z, t)$, such that

$$\boldsymbol{u} = \boldsymbol{\nabla}\phi_l. \tag{2.1}$$

The fluid is assumed inviscid and barotropic. Compressibility effects are characterised by the dimensionless parameter

$$\mu = \frac{gh}{c^2} \ll 1, \tag{2.2}$$

which compares the characteristic gravity-wave speed $\sqrt{gh}$ with the sound speed c, which is assumed to be constant; the parameter g is the acceleration due to gravity. This parameter naturally governs acoustic–gravity interactions in surface-wave problems (Longuet-Higgins 1950; Kadri & Stiassnie 2013).

For completeness, we present the fully nonlinear compressible potential-flow equation and the free-surface conditions that underlie the weakly nonlinear triad reduction. Combining continuity with Bernoulli yields the nonlinear interior equation (cf. Longuet-Higgins 1950; Kadri & Akylas 2016)

$$\phi_{l,tt} - c^2\boldsymbol{\nabla}^2\phi_l - \partial_t\left(\frac{1}{2}|\boldsymbol{\nabla}\phi_l|^2\right) - \frac{1}{2}\boldsymbol{u}\cdot\boldsymbol{\nabla}\left(|\boldsymbol{\nabla}\phi_l|^2\right) = 0, \qquad -h \leqslant z \leqslant 0. \tag{2.3}$$

In addition, the standard kinematic and dynamic boundary conditions apply at the free surface $z = \eta(x, t)$. For the weakly nonlinear analysis that follows, it is sufficient to enforce these conditions consistently through cubic order in the perturbation expansion. Expanding the exact kinematic and dynamic conditions about the mean level $z = 0$ and eliminating η order by order yields the following combined boundary condition for ϕ_l:

$$\begin{aligned}\phi_{l,tt} + g\phi_{l,z} + \frac{1}{c^2}\partial_t\left(|\boldsymbol{\nabla}\phi_l|^2\right) - \partial_z\left[\frac{1}{c^2}\phi_{l,t}\left(\phi_{l,tt} + g\phi_{l,z}\right)\right] + \frac{1}{2c^2}\boldsymbol{u}\cdot\boldsymbol{\nabla}\left(|\boldsymbol{\nabla}\phi_l|^2\right)\\ - \partial_z\left[\frac{1}{c^2}\phi_{l,t}\partial_t\left(|\boldsymbol{\nabla}\phi_l|^2\right)\right] - \frac{1}{2}\partial_z\left[\left(\phi_{l,tt} + g\phi_{l,z}\right)\left(\frac{1}{c^2}|\boldsymbol{\nabla}\phi_l|^2 - \frac{1}{c^4}\phi_{l,t}^2\right)\right] = 0, \qquad z = 0.\end{aligned} \tag{2.4}$$

https://doi.org/10.1017/jfm.2026.11735 Published online by Cambridge University Press

In non-dimensional variables this combined condition (2.4) is given explicitly by (3.2*a*) of Kadri & Akylas (2016). In the present dimensional variables it can be written compactly as

$$\phi_{l,tt} + g\phi_{l,z} = \varepsilon \mathcal{N}_2[\phi_l] + \varepsilon^2 \mathcal{N}_3[\phi_l] \qquad (z = 0), \tag{2.5}$$

where ε is the small wave-steepness/nonlinearity parameter, $\mathcal{N}_2$ and $\mathcal{N}_3$ are the standard quadratic and cubic free-surface operators arising from the Taylor expansion and elimination of η (Phillips 1960; Craik 1985), and for the triad ordering adopted here they coincide with those used in Kadri & Akylas (2016).

Under weakly compressible conditions, the compressible potential-flow equations may be expanded asymptotically in μ. To leading order in the bulk, the velocity potential satisfies the linear acoustic-wave equation

$$\phi_{l,tt} - c^2 \nabla^2 \phi_l = 0, \qquad -h \leqslant z \leqslant 0, \tag{2.6}$$

while nonlinear compressibility effects in the interior appear at higher order (Longuet-Higgins 1950; Kadri & Akylas 2016). The bulk formulation can be written with or without an added $g\phi_{l,z}$ term depending on the potential convention (see, e.g. Longuet-Higgins 1950); we adopt the convention consistent with Kadri & Akylas (2016) and with the elastic-bottom eigenproblem in Eyov *et al.* (2013).

At the free surface $z = \eta(x, t)$, the exact kinematic and dynamic boundary conditions apply. Linearisation yields the combined free-surface condition

$$\phi_{l,tt} + g\phi_{l,z} = 0, \qquad z = 0. \tag{2.7}$$

In the weakly nonlinear derivation in § 5, the full kinematic and dynamic free-surface conditions at $z = \eta(x, t)$ are expanded consistently through $O(\varepsilon^3)$ following standard procedures (Phillips 1960; Craik 1985; Kadri & Akylas 2016). For brevity, we display only the linear combined condition (2.7) here, while the quadratic and cubic contributions enter the $O(\varepsilon^3)$ problem through the forcing terms introduced in § 5.4.

2.2. *Elastic half-space*

The fluid overlies an elastic half-space occupying $z \leqslant -h$, assumed homogeneous, isotropic and linearly elastic. The solid is characterised by density ρ_s and Lamé parameters λ_s and μ_s, or equivalently by the compressional and shear wave speeds

$$C_p = \sqrt{\frac{\lambda_s + 2\mu_s}{\rho_s}}, \qquad C_s = \sqrt{\frac{\mu_s}{\rho_s}}. \tag{2.8}$$

Elastic coupling at a fluid–solid interface is known to modify both acoustic and gravity-wave propagation (Biot 1952). Following standard treatments in hydroacoustics and elastic-wave theory (Achenbach 1973; Eyov *et al.* 2013), we impose at $z = -h$ continuity of vertical velocity and normal traction, together with vanishing shear traction. Eliminating the elastic variables yields an effective boundary condition acting on the fluid potential

$$\mathcal{B}_e(\omega, \kappa)[\phi_l] \equiv \phi_{l,z} - \mathcal{Z}(\omega, \kappa)\phi_l = 0, \qquad z = -h, \tag{2.9}$$

where $\mathcal{Z}(\omega, \kappa)$ is an impedance function determined by the elastic properties of the half-space (see Appendix A for the explicit expression). Here ω denotes angular frequency and κ the horizontal wavenumber of the acoustic–gravity mode.

A central point for what follows is that the bottom operator $\mathcal{B}_e$ depends explicitly on the spectral parameters (ω, κ) through $\mathcal{Z}(\omega, \kappa)$. This explicit dependence is responsible for an additional interfacial contribution in the weakly nonlinear solvability condition derived

https://doi.org/10.1017/jfm.2026.11735 Published online by Cambridge University Press

in § 5. In the rigid-bottom limit one has $\mathcal{Z} \to 0$, so that (2.9) reduces to the classical no-penetration condition $\phi_{l,z} = 0$ at $z = -h$.

Note that $\mathcal{Z}(\omega, \kappa)$ depends smoothly on (ω, κ) in the neighbourhood of the resonant acoustic–gravity mode. Thus, the impedance does not alter the structure of the weakly nonlinear theory; it only affects the coefficient values through $\mathcal{Z}$ and its derivatives evaluated on the resonant branch.

3. Linear acoustic–gravity modes over an elastic half-space

The compressional member of the triad is a finite-depth acoustic–gravity eigenmode of the coupled fluid–solid system. It is acoustic in the bulk (governed by the compressible wave equation) and gravity coupled through the free-surface boundary condition. For brevity we occasionally refer to this mode as the acoustic mode in the triad equations; in all such instances it is the acoustic–gravity branch defined by the elastic half-space dispersion relation.

In the sequel we examine the linear acoustic–gravity modes supported by the coupled fluid–elastic solid system. These modes form the basis for the weakly nonlinear triad analysis in § 5.

3.1. *Eigenvalue problem and explicit eigenfunction*

We seek time-harmonic solutions

$$\phi_l(x, z, t) = \Phi(z) \mathrm{e}^{\mathrm{i}(\kappa x - \omega t)} + \text{c.c.}, \tag{3.1}$$

where κ is the horizontal wavenumber, ω is the (angular) frequency of the acoustic–gravity mode in the coupled fluid–solid system, and c.c. denotes the complex conjugate. For progressive non-evanescent acoustic modes κ is both real and positive. The bulk (2.6) yields

$$\Phi_{zz} + \alpha^2 \Phi = 0, \qquad \alpha^2 = \frac{\omega^2}{c^2} - \kappa^2, \qquad -h \leqslant z \leqslant 0. \tag{3.2}$$

We take the branch $\alpha = \sqrt{\omega^2/c^2 - \kappa^2}$ with $\Re(\alpha) \geqslant 0$. When α is real the vertical structure in the fluid is oscillatory (propagating acoustic–gravity mode), whereas $\alpha = \mathrm{i}|\alpha|$ corresponds to evanescence in z, i.e. gravity mode. The linear free-surface condition (2.7) becomes

$$g\Phi_z - \omega^2 \Phi = 0, \qquad z = 0, \tag{3.3}$$

while the elastic solid interface condition (2.9) becomes

$$\Phi_z - \mathcal{Z}(\omega, \kappa)\Phi = 0, \qquad z = -h. \tag{3.4}$$

Solving (3.2) subject to (3.4) gives the explicit representation

$$\Phi_e(z) = C\left[\cos\alpha(z + h) + \frac{\mathcal{Z}(\omega, \kappa)}{\alpha} \sin\alpha(z + h)\right], \qquad -h \leqslant z \leqslant 0, \tag{3.5}$$

so that $\Phi_e(-h) = C$. A convenient normalisation is $\Phi_e(0) = 1$, giving

$$C = \left[\cos(\alpha h) + \frac{\mathcal{Z}(\omega, \kappa)}{\alpha} \sin(\alpha h)\right]^{-1}. \tag{3.6}$$

https://doi.org/10.1017/jfm.2026.11735 Published online by Cambridge University Press

3.2. *Elastic solid dispersion relation and rigid limit*

Imposing the free-surface condition (3.3) on (3.5) yields the elastic solid dispersion relation (see Appendix A)

$$D_e(\omega, \kappa; h) \equiv g\Big[-\alpha \sin(\alpha h) + \mathcal{Z}(\omega, \kappa)\cos(\alpha h)\Big] - \omega^2\Big[\cos(\alpha h) + \frac{\mathcal{Z}(\omega, \kappa)}{\alpha}\sin(\alpha h)\Big] = 0. \tag{3.7}$$

In the rigid-bottom limit $\mathcal{Z} \to 0$, (3.7) reduces to

$$D_r(\omega, \kappa; h) \equiv -g\alpha \sin(\alpha h) - \omega^2 \cos(\alpha h) = 0, \tag{3.8}$$

which is the classical rigid-bottom acoustic–gravity dispersion relation used in previous triad analyses. It will be useful later to write

$$D_e(\omega, \kappa; h) = D_r(\omega, \kappa; h) + \mathcal{Z}(\omega, \kappa) Q(\omega, \kappa; h), \tag{3.9}$$

where the multiplier Q is explicitly

$$Q(\omega, \kappa; h) = g\cos(\alpha h) - \frac{\omega^2}{\alpha}\sin(\alpha h). \tag{3.10}$$

3.3. *Cutoff and admissibility: rigid versus elastic bottoms*

In the present lossless setting we focus on real (ω, κ) solutions of the dispersion relations. Under rigid-bottom conditions, admissible propagating acoustic–gravity modes correspond to real roots of $D_r(\omega, \kappa; h) = 0$ with real α (equivalently $\omega^2/c^2 > \kappa^2$), while $\alpha = \mathrm{i}|\alpha|$ yields evanescent vertical structure. In shallow configurations, the rigid-bottom acoustic–gravity branch may terminate in the sense that $D_r(\omega, \kappa; h) = 0$ admits no real propagating roots for given (ω, κ); this is the rigid cutoff referred to in earlier triad analyses.

A convenient mathematical characterisation of a cutoff point $(\omega_c, \kappa_c; h_c)$ is a turning-point (degeneracy) condition

$$D_r(\omega_c, \kappa_c; h_c) = 0, \qquad \partial_\omega D_r(\omega_c, \kappa_c; h_c) = 0, \tag{3.11}$$

at which the propagating branch ceases to continue as a real-valued function of depth (or frequency). Physically, the rigid no-penetration condition inhibits vertical motion at $z = -h$ and can prevent the existence of a trapped propagating acoustic–gravity mode when the water column is too shallow, so that the acoustic member of the triad becomes evanescent and resonance cannot be satisfied with real (ω, κ).

For the first rigid acoustic–gravity branch, a simple way to view the cutoff is to note that in the rigid limit the vertical structure must satisfy a node/antinodal constraint imposed by $\Phi_z = 0$ at $z = -h$ together with the free-surface condition at $z = 0$. When the water column is too shallow, these constraints cannot be satisfied by a real (oscillatory) vertical wavenumber α at a prescribed frequency, so the admissible propagating root disappears and the mode becomes vertically evanescent. In particular, for $\kappa \approx 0$ the first cutoff occurs near $\alpha h = \pi/2$, giving the classical estimate $\omega_c \approx \pi c/(2h)$ used in figure 1 (also see Stiassnie 2010).

Elastic solid coupling modifies admissibility through the impedance condition (3.4), which changes the boundary-value problem and hence the dispersion relation (3.7). In particular, the coupled system may admit propagating or interface-guided acoustic–gravity modes (with energy shared between the fluid and the solid) in parameter regimes where the rigid problem supports only evanescence. This extension of the admissible spectrum is the primary mechanism by which elasticity enlarges the parameter space of resonant triads

https://doi.org/10.1017/jfm.2026.11735 Published online by Cambridge University Press

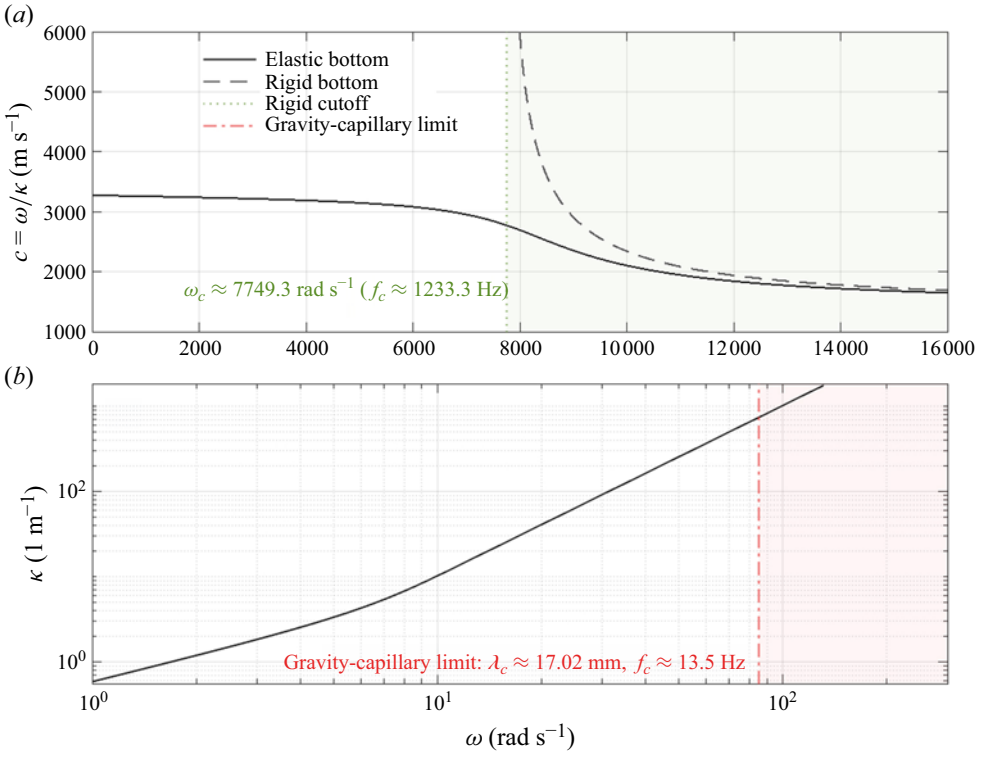


Figure 1. Rigid-bottom versus elastic-bottom acoustic–gravity dispersion at $h = 0.30$, m (parameters in § 3.4). (*a*) Phase speed ω/κ versus ω for the first acoustic–gravity branch: the rigid-bottom mode (dashed) exists only for $\omega > \omega_c = \pi c/(2h)$ (vertical dotted line), whereas elastic coupling (solid) supports an interface-guided branch below ω_c. (*b*) Elastic branch shown as $\kappa(\omega)$ on logarithmic axes in the laboratory-relevant low-frequency range; the vertical dash-dotted line marks the gravity–capillary cross-over ω_{gc}.

and, in the examples below, removes the rigid cutoff in frequency (or depth) relevant to shallow-water and laboratory-scale configurations.

3.4. *Illustrative shallow-water parameters and dispersion comparison*

To quantify frequency scales relevant to admissibility at laboratory depths, we take $h = 0.30$ m and the water–elastic solid half-space parameters used by Eyov *et al.* (2013): $c = 1480\,\mathrm{m\,s^{-1}}$ and $\rho_l = 1000\,\mathrm{kg\,m^{-3}}$ in the fluid, over a stiff (granite-like) elastic solid half-space with $\rho_s = 2750\,\mathrm{kg\,m^{-3}}$, $C_s = 3550\,\mathrm{m\,s^{-1}}$ and $C_p = 6300\,\mathrm{m\,s^{-1}}$. For these values, the weak-compressibility parameter is $\mu = gh/c^2 \approx 1.3 \times 10^{-6}$.

At this depth the rigid-bottom acoustic–gravity branch is effectively inaccessible in the laboratory-frequency band: the classical rigid cutoff $\omega_c = \pi c/(2h) \approx 7.75 \times 10^3$ rad s^{-1} (equivalently $f_c \approx 1.23$ kHz) lies far above typical gravity-wave forcing frequencies $O(1)$–$O(10)$ Hz. This is evident in figure 1(*a*), where the rigid mode (dashed) appears only for $\omega > \omega_c$, whereas elastic solid coupling supports an interface-guided branch (solid) that continues smoothly below ω_c and therefore admits a propagating acoustic–gravity participant in the laboratory regime. The low-frequency behaviour of this elastic solid branch is highlighted in figure 1(*b*), which plots $\kappa(\omega)$ on logarithmic axes over the experimentally relevant range. In particular, the elastic solid branch persists below the gravity–capillary cross-over $\omega_{gc} \approx 85.1$ rad, s^{-1} ($f_{gc} \approx 13.5$ Hz), so the surface-wave components can remain ordinary gravity waves while the acoustic–gravity member

https://doi.org/10.1017/jfm.2026.11735 Published online by Cambridge University Press

remains admissible. Together, figures 1(*a*) and 1(*b*) illustrate the key experimental implication: elasticity removes the rigid-bottom cutoff obstruction and makes triad configurations feasible at laboratory scales, without the need to enter the gravity-capillary regime.

4. Resonant triads and admissibility conditions

We now identify the class of resonant (or weakly detuned) triads that can arise in the coupled fluid–elastic solid system and examine how elasticity modifies their admissibility. The analysis closely parallels the rigid-bottom case, but with important differences arising from the elastic modification of the acoustic–gravity wave spectrum.

4.1. *Triad structure*

We consider resonant interactions involving two free-surface gravity waves and one acoustic–gravity wave. The two surface wavetrains are taken to be nearly monochromatic, with (possibly distinct) horizontal wavenumbers k_+ and k_- and corresponding frequencies ω_+ and ω_-. The third member of the triad is an acoustic–gravity mode with horizontal wavenumber κ and frequency ω.

Resonance requires approximate satisfaction of the wavenumber- and frequency-matching conditions

$$k_+ + k_- = \kappa, \qquad \omega_+ + \omega_- = \omega - \mu\beta, \tag{4.1}$$

where $\beta = O(1)$ measures detuning, where $\beta = 0$ corresponds to exact resonance. The resonance conditions (4.1) are written for a two-dimensional, long-crested setting in which all waves share the same horizontal direction x; hence only the horizontal wavenumbers appear. Energy exchange with the elastic half-space does not require an additional horizontal component: it is mediated by the vertical eigenstructure and the impedance condition at $z = -h$, which couples the fluid pressure field to evanescent (or guided) elastic fields in the substrate.

The detuning is written as $\mu\beta$ because the interaction is studied on the slow time $T = \mu t$ (with $\varepsilon \sim \mu^{1/2}$), so only an $O(\mu)$ frequency mismatch produces an $O(1)$ phase drift on the modulation time scale. In the nearly counter-propagating configuration of primary interest, $k_+ \approx -k_-$ so that $\kappa = k_+ + k_-$ is small compared with $|k_\pm|$, consistent with the long horizontal scale of the acoustic–gravity member. Other triad geometries are possible in principle, but the near counter-propagating case is the most relevant for laboratory forcing and for the classic microseism setting where two opposing surface wavetrains generate the compressional response.

4.2. *Admissibility under rigid and elastic bottoms*

Under rigid-bottom conditions, the admissibility of acoustic–gravity triads is constrained by the dispersion relation of the acoustic mode. In shallow water, the acoustic–gravity branch may become evanescent, or cease to exist altogether as a propagating mode. In such cases, the resonance conditions (4.1) cannot be satisfied with real ω and κ, and the triad interaction is suppressed.

By altering the dispersion relation $\omega(\kappa)$ of the acoustic–gravity mode, elastic coupling modifies the above picture in two distinct ways. First, it allows for new propagating elastic or interface-guided modes that become admissible in parameter regimes where the rigid-bottom problem supports only evanescent solutions. Second, it changes the set of wavenumber pairs (k_+, k_-) for which resonance is possible.

https://doi.org/10.1017/jfm.2026.11735 Published online by Cambridge University Press

As a result, elasticity enlarges the admissible parameter space for resonant triads, particularly in shallow-water configurations. This observation has important implications for both laboratory experiments and field-scale applications, as it suggests that elastic substrates can be used to tune the system into resonance without requiring large fluid depths.

5. Weakly nonlinear theory and elastic solvability condition

In this section we derive the evolution equations governing resonant acoustic–gravity wave triads over an elastic half-space. The analysis follows the weakly nonlinear multiple-scale framework developed by Kadri & Akylas (2016) for rigid-bottom configurations, with the essential modification that the acoustic–gravity eigenproblem now involves an elastic boundary operator. Because this operator depends explicitly on the spectral parameters, the solvability condition acquires an additional interface contribution.

5.1. *Multiple-scale expansion*

We introduce a small wave-steepness parameter $\varepsilon \ll 1$ and expand the velocity potential as

$$\phi_l = \varepsilon\phi^{(1)} + \varepsilon^2\phi^{(2)} + \varepsilon^3\phi^{(3)} + \cdots . \tag{5.1}$$

Slow modulation associated with near-resonant interactions is captured by the slow time T, and we adopt the distinguished scaling $\varepsilon \sim \mu^{1/2}$, which ensures that quadratic nonlinear forcing balances slow-time modulation at leading order (Kadri & Akylas 2016). Under this ordering, nonlinear terms in the bulk equations are asymptotically smaller than the nonlinear contributions arising from the free-surface boundary condition. Consequently, at the order relevant to triad resonance the interior correction is governed by the homogeneous linear equation associated with the acoustic–gravity eigenproblem, while nonlinearity enters through the free-surface boundary conditions and appears as resonant forcing at $O(\varepsilon^3)$. To allow for weak spatial modulation, we also introduce the slow horizontal variable $X = \mu^2 x$, and hence take the wave envelopes to depend on (X, T). Accordingly, derivatives act as

$$\partial_t \mapsto \partial_t + \mu\partial_T, \qquad \partial_x \mapsto \partial_x + \mu^2\partial_X, \tag{5.2}$$

where ∂_t, ∂_x on the right-hand side denote differentiation with respect to fast scales, and ∂_T, ∂_X represent differentiation with respect to slow scales.

5.2. *Leading-order solution*

At $O(\varepsilon)$, the solution is taken as a superposition of two surface gravity wavetrains and one acoustic–gravity mode

$$\phi^{(1)} = \phi_g^+ + \phi_g^- + \phi_e. \tag{5.3}$$

The gravity-wave components are written as

$$\phi_g^\pm = S_\pm(X, T)\Phi_g^\pm(z)\mathrm{e}^{\mathrm{i}(k_\pm x - \omega_\pm t)} + \text{c.c.}, \tag{5.4}$$

where $S_\pm(X, T)$ are slowly varying complex amplitudes. For each wavetrain, the vertical structure $\Phi_g^\pm(z)$ is the standard linear gravity-wave eigenfunction associated with $(k_\pm, \omega_\pm)$ for the chosen depth and bottom model. In the nearly counter-propagating configuration of interest, $k_+ \approx -k_-$ and the two gravity-wave frequencies are close, but they are not assumed identical *a priori*. In the weakly compressible regime $\mu \ll 1$,

https://doi.org/10.1017/jfm.2026.11735 Published online by Cambridge University Press

and following Kadri & Akylas (2016), we take the two surface gravity wavetrains to be the classical incompressible deep-water modes. Accordingly, $\Phi_g^{\pm}$ satisfy the standard Laplace eigenproblem in $z < 0$ with the linear free-surface condition at $z = 0$ and decay as $z \to -\infty$. For consistency with the finite-depth coupled problem, we assume $k_{\pm}h \gg 1$, so that the gravity-wave eigenfunctions are exponentially small at $z = -h$ and bottom compliance affects $\phi_g^{\pm}$ only beyond the order retained; elasticity is therefore retained only in the acoustic–gravity eigenproblem that closes the triad. More precisely, taking $k_{\pm}h = O(1/\mu) \gg 1$ gives $\Phi_g^{\pm}(-h) = O(\mathrm{e}^{-|k_{\pm}|h}) = O(\mathrm{e}^{-1/\mu})$, so seabed (bottom boundary) elasticity modifies the gravity-wave dispersion/structure only at exponentially small order, beyond the $O(\mu)$ accuracy retained here. Accordingly, the surface-wave frequencies satisfy the deep-water dispersion relation

$$\omega_{\pm}^2 = g|k_{\pm}|, \tag{5.5}$$

and the corresponding vertical structure may be taken as $\Phi_g^{\pm}(z) \propto \mathrm{e}^{|k_{\pm}|z}$ in the fluid region.

The acoustic–gravity component is written as

$$\phi_e = A(X, T)\Phi_e(z)\mathrm{e}^{\mathrm{i}(\kappa x - \omega t)} + \text{c.c.}, \tag{5.6}$$

where $A(X, T)$ is the slowly varying amplitude of the acoustic–gravity mode and $\Phi_e(z)$ satisfies the elastic eigenvalue problem derived in § 3. Here, the complex envelopes $S_{\pm}$ and A vary on the slow scales (X, T).

5.3. *Second-order fields*

At $O(\varepsilon^2)$, the governing equations are forced by quadratic products of the leading-order fields. The resulting solution consists of bound waves and non-resonant components. No secular terms arise at this order, and the explicit form of $\phi^{(2)}$ is not required; only its contribution to resonant forcing at $O(\varepsilon^3)$ enters the amplitude equations.

5.4. *Third-order problem and solvability condition*

At $O(\varepsilon^3)$ the governing equations admit resonant forcing at the acoustic–gravity phase $\mathrm{e}^{\mathrm{i}(\kappa x - \omega t)}$. The corresponding correction is written as

$$\phi^{(3)} = F(z)\mathrm{e}^{\mathrm{i}(\kappa x - \omega t)} + \text{c.c.}, \tag{5.7}$$

where $F(z)$ satisfies the forced boundary-value problem

$$F_{zz} + \alpha^2 F = R_1(z), \qquad -h < z < 0. \tag{5.8}$$

Here, $R_1(z)$ collects quadratic products of the leading-order fields and contributions arising from slow-time modulation.

At the free surface $z = 0$, the inhomogeneous boundary condition takes the form

$$\left(gF_z - \omega^2 F\right)\big|_{z=0} = R_2, \tag{5.9}$$

where R_2 arises from quadratic free-surface nonlinearities and from slow-time derivatives.

Since $\mathcal{B}_e$ depends explicitly on the spectral parameters, the boundary operator acquires an $O(\mu)$ correction from the same slow detuning already introduced in the resonance condition (4.1). Thus, rather than introducing a separate corrected frequency, we let the mismatch enter through the acoustic-phase forcing at frequency $\omega - \mu\beta$, where $\beta = O(1)$ is the detuning parameter. Linearising the elastic boundary operator about the resonant

https://doi.org/10.1017/jfm.2026.11735 Published online by Cambridge University Press

acoustic–gravity mode then gives

$$\mathcal{B}_e(\omega-\mu\beta,\kappa)[\Phi_e+\mu F]=\mathcal{B}_e(\omega,\kappa)[\Phi_e]+\mu\mathcal{B}_e(\omega,\kappa)[F]-\mu\beta\,(\partial_\omega\mathcal{B}_e)\,(\omega,\kappa)[\Phi_e]+O(\mu^2). \tag{5.10}$$

Since $\mathcal{B}_e(\omega,\kappa)[\Phi_e]=0$ by the linear eigenproblem, the $O(\mu)$ balance yields the effective boundary condition for F

$$F_z-\mathcal{Z}(\omega,\kappa)F=-\beta\,\partial_\omega\mathcal{Z}(\omega,\kappa)\Phi_e,\qquad z=-h, \tag{5.11}$$

or equivalently

$$\mathcal{B}_e(\omega,\kappa)[F]=\beta\,(\partial_\omega\mathcal{B}_e(\omega,\kappa))\,[\Phi_e], \tag{5.12}$$

since $\mathcal{B}_e(\omega,\kappa)[\phi]=\phi_z-\mathcal{Z}(\omega,\kappa)\phi$.

For fixed (ω,κ) and real (lossless) impedance, the vertical Sturm–Liouville operator with the boundary condition (3.4) is self-adjoint under the standard inner product, so the adjoint eigenfunction is proportional to Φ_e. Multiplying (5.8) by Φ_e, subtracting the homogeneous equation multiplied by F and integrating by parts over $-h<z<0$ yields the Green-type identity

$$\int_{-h}^{0}\Phi_e R_1\,\mathrm{d}z=\Big[\Phi_e F_z-\Phi_{e,z}F\Big]_{-h}^{0}. \tag{5.13}$$

The contribution at the free surface reduces to

$$\Big(\Phi_e F_z-\Phi_{e,z}F\Big)\Big|_{z=0}=\frac{1}{g}\Phi_e(0)R_2, \tag{5.14}$$

which coincides with the rigid-bottom case.

Using (5.11) in the boundary term of the Green identity shows that the interface contribution does not vanish and is proportional to the slow detuning

$$-\Big(\Phi_e F_z-\Phi_{e,z}F\Big)\Big|_{z=-h}=\mathcal{I}_e, \tag{5.15}$$

where

$$\mathcal{I}_e=\beta\big(\partial_\omega\mathcal{B}_e(\omega,\kappa)\big)[\Phi_e]\Phi_e(-h), \tag{5.16}$$

where $\beta=O(1)$ is the same detuning parameter introduced in the resonance condition (4.1), so that the actual frequency mismatch enters at order $\mu\beta$ on the slow modulation time scale. Any contribution proportional to $\partial_\kappa\mathcal{B}_e$ can arise only through spatial modulation of the phase, i.e. through $\kappa=\kappa_0+O(\mu^2)$ induced by dependence on $X=\mu^2x$. Under this distinguished scaling, the resulting $\partial_\kappa\mathcal{B}_e$ term enters one order higher than the $O(\mu)$ detuning contribution and is therefore neglected at the present order.

The solvability condition governing resonant-triad interactions over an elastic half-space thus takes the form

$$\int_{-h}^{0}\Phi_e R_1\,\mathrm{d}z=\frac{1}{g}\Phi_e(0)R_2+\mathcal{I}_e. \tag{5.17}$$

5.5. *Triad equations and elastic normalisation*

The solvability condition (5.17) provides the slow-time evolution of the acoustic–gravity amplitude $A(X,T)$ and the two gravity-wave envelopes $S_\pm(X,T)$. The passage from (5.17) to the modulation system is standard: after extracting the coefficients of $\mathrm{e}^{\mathrm{i}(\kappa x-\omega t)}$ in R_1 and R_2, the slow-time terms generated by $\partial_t\mapsto\partial_t+\mu\partial_T$ produce the factor $\mathcal{N}_e\partial_T A$,

https://doi.org/10.1017/jfm.2026.11735 Published online by Cambridge University Press

while the quadratic interaction of the two gravity waves produces the forcing term $\mathcal{P}S_+S_-$. Carrying out the analogous projection for the gravity-wave phases yields the coupled system (5.18). The detuning parameter β is the same $O(\mu)$ frequency mismatch introduced in (4.1). The modulation equations take the canonical resonant-triad form with weak spatial modulation

$$\partial_T A + c_e \partial_X A = \mathrm{i}\gamma_e A + \delta_e S_+ S_-, \tag{5.18a}$$

$$\partial_T S_\pm + c_{g\pm} \partial_X S_\pm = -\frac{\delta_e}{2} A S_\mp^*. \tag{5.18b}$$

Here, $c_{g\pm} = \partial\omega_\pm/\partial k_\pm$ are the group velocities of the two surface gravity wavetrains (for the chosen depth and bottom model), and $c_e = \partial\omega/\partial\kappa$ is the group velocity of the elastic acoustic–gravity mode, with $\omega = \omega(\kappa)$ determined implicitly by the elastic dispersion relation $D_e(\omega, \kappa; h) = 0$. In particular, differentiating $D_e(\omega(\kappa), \kappa; h) = 0$ yields

$$c_e = \frac{\partial\omega}{\partial\kappa} = -\frac{\partial_\kappa D_e}{\partial_\omega D_e}, \tag{5.19}$$

evaluated on the acoustic–gravity branch.

The detuning parameter β is the same $O(\mu)$ frequency mismatch introduced in (4.1). It enters the acoustic-mode equation as an additive phase-mismatch contribution, so that

$$\delta_e = \frac{\mathcal{P}}{\mathcal{N}_e}, \qquad \gamma_e = \frac{\mathcal{D}}{\mathcal{N}_e} + \beta, \tag{5.20}$$

where $\mathcal{P}$ is the quadratic projection of the gravity–gravity forcing onto the acoustic mode and $\mathcal{D}$ collects linear dispersive corrections. For completeness, the coefficients $\mathcal{P}$ and $\mathcal{D}$ can be written directly in terms of the resonant forcing in (5.8)–(5.9). In the lossless case considered here the vertical operator is self-adjoint, so the adjoint mode may be taken as Φ_e^* (and $\Phi_e^* = \Phi_e$ for real eigenfunctions). Denoting by $R_1^{(res)}(z)$ and $R_2^{(res)}$ the components of (R_1, R_2) proportional to $\mathrm{e}^{\mathrm{i}(\kappa x - \omega t)}$, we define

$$\begin{aligned}
\mathcal{P} &= \int_{-h}^{0} \Phi_e^*(z) R_1^{(\mathrm{res})}(z)\mathrm{d}z + \frac{1}{g}\Phi_e^*(0) R_2^{(\mathrm{res})}, \\
\mathcal{D} &= \int_{-h}^{0} \Phi_e^*(z) R_1^{(disp)}(z)\mathrm{d}z + \frac{1}{g}\Phi_e^*(0) R_2^{(disp)},
\end{aligned} \tag{5.21}$$

where $(R_1^{(disp)}, R_2^{(disp)})$ denote the parts of the $O(\varepsilon^3)$ forcing generated by slow modulation (including the T-derivative terms) and other linear dispersive corrections on the chosen scaling. Elasticity enters the triad dynamics only through the acoustic-mode normalisation $\mathcal{N}_e$. With the eigenfunction $\Phi_e(z)$ normalised by $\Phi_e(0) = 1$, the normalisation decomposes as

$$\mathcal{N}_e = \mathcal{N}_{fs} + \mathcal{N}_{int}, \tag{5.22}$$

where the classical free-surface contribution is

$$\mathcal{N}_{fs} = \int_{-h}^{0} \frac{2\omega}{c^2}|\Phi_e(z)|^2\mathrm{d}z + \frac{2\omega}{g}|\Phi_e(0)|^2 = \int_{-h}^{0} \frac{2\omega}{c^2}|\Phi_e(z)|^2\mathrm{d}z + \frac{2\omega}{g}, \tag{5.23}$$

and the elastic interface contribution, arising from the explicit (ω, κ)-dependence of the impedance boundary operator (2.9), is

$$\mathcal{N}_{int} = 2\omega \frac{\partial \mathcal{Z}}{\partial\omega}(\omega, \kappa)|\Phi_e(-h)|^2. \tag{5.24}$$

https://doi.org/10.1017/jfm.2026.11735 Published online by Cambridge University Press

The term $\mathcal{N}_{int}$ is the direct counterpart of the interface contribution $\mathcal{I}_e$ in (5.16) for impedance-type boundary conditions. In the rigid-bottom limit $\mathcal{Z} \to 0$ smoothly (hence $\partial_\omega \mathcal{Z} \to 0$), so $\mathcal{N}_{int} \to 0$ and $\mathcal{N}_e \to \mathcal{N}_{fs}$.

5.6. *Dispersion-derivative identity*

An equivalent characterisation of the normalisation follows directly from the elastic dispersion relation $D_e(\omega, \kappa; h) = 0$. Differentiating D_e with respect to ω, and using the homogeneous eigenproblem for Φ_e, yields the identity

$$\mathcal{N}_e = \frac{1}{2\omega} \frac{\partial D_e}{\partial \omega}(\omega, \kappa; h). \tag{5.25}$$

Here, $\partial_\omega D_e$ denotes differentiation with respect to ω holding κ fixed, and the result is evaluated on the acoustic–gravity branch satisfying $D_e(\omega, \kappa; h) = 0$. This is convenient for analysis and confirms that elasticity modifies the triad coefficients through the same object that controls the sensitivity of the acoustic branch to frequency.

6. Energetics and elastic partition of the acoustic mode

The triad evolution equations describe slow-time exchange between two surface gravity wavetrains and a single acoustic–gravity mode supported by the coupled fluid–solid system. It is therefore useful to distinguish between (i) quadratic invariants of the modulation system and (ii) the physical partition of acoustic-mode energy between the fluid and the elastic half-space.

6.1. *A conserved quadratic invariant*

With weak spatial modulation, the triad system (5.18) possesses a local conservation law. To see this, multiply the acoustic equation by A^*, add its complex conjugate, and use

$$\partial_T (A^* A) + c_e \partial_X (A^* A) = A^* \big(\mathrm{i}\gamma_e A + \delta_e S_+ S_- \big) + A \big(-\mathrm{i}\gamma_e^* A^* + \delta_e^* S_+^* S_-^* \big). \tag{6.1}$$

This gives

$$\partial_T \big(|A|^2 \big) + c_e \partial_X \big(|A|^2 \big) = 2\Re \left(\delta_e A^* S_+ S_- \right), \tag{6.2}$$

where the detuning term contributes only an imaginary part and hence does not affect the balance. Similarly, multiplying the gravity-wave equations by $S_\pm^*$ and adding complex conjugates yields

$$\partial_T \big(|S_\pm|^2 \big) + c_{g\pm} \partial_X \big(|S_\pm|^2 \big) = -\Re \left(\delta_e A^* S_+ S_- \right). \tag{6.3}$$

Summing (6.2) and the two relations (6.3) gives the local conservation law

$$\partial_T \left(|A|^2 + |S_+|^2 + |S_-|^2 \right) + \partial_X \left(c_e |A|^2 + c_{g+} |S_+|^2 + c_{g-} |S_-|^2 \right) = 0. \tag{6.4}$$

In particular, if the envelopes are periodic in X or decay sufficiently rapidly as $|X| \to \infty$, then integration over X shows that $\int (|A|^2 + |S_+|^2 + |S_-|^2) \mathrm{d}X$ is conserved. This 'action-like' conservation law is a standard property of resonant triads and follows from the canonical structure of the modulation equations. It does not, by itself, specify how the acoustic-mode physical energy is distributed between the fluid and the solid.

6.2. *Physical acoustic-mode energy and elastic partition*

The physical quadratic energy associated with the acoustic–gravity mode is proportional to the normalisation arising from the solvability condition. With the eigenfunction

https://doi.org/10.1017/jfm.2026.11735 Published online by Cambridge University Press

normalised by $\Phi_e(0) = 1$, the mode energy may be written (up to a constant prefactor) as

$$E_e^{phys} \propto (\mathcal{N}_{fs} + \mathcal{N}_{int})|A|^2, \tag{6.5}$$

where $\mathcal{N}_{fs}$ and $\mathcal{N}_{int}$ are given explicitly by (5.23)–(5.24). For impedance conditions of the form $\phi_{l,z} - \mathcal{Z}(\omega, \kappa)\phi_l = 0$, the interface contribution to the frequency normalisation arises from the ω-sensitivity of the boundary operator (equivalently, from $\partial_\omega D_e$), while κ-dependence enters the detuning/dispersion corrections through the elastic dispersion relation $D_e(\omega, \kappa; h)$ and is accounted for in $\mathcal{D}$ and β. This decomposition provides a natural energetic interpretation

$$E_{e,f}^{phys} \propto \mathcal{N}_{fs}|A|^2, \qquad E_{e,s}^{phys} \propto \mathcal{N}_{int}|A|^2, \tag{6.6}$$

where $E_{e,f}^{phys}$ is the fluid-associated contribution (bulk plus free surface), while $E_{e,s}^{phys}$ measures the portion of the acoustic-mode energy stored in (or transmitted into) the elastic half-space through the impedance operator.

In the rigid-bottom limit $\mathcal{Z} \to 0$, $\mathcal{N}_{int} \to 0$ and the acoustic-mode energy is entirely contained in the fluid. For an elastic half-space, $\mathcal{N}_{int}$ is generally non-zero and quantifies the degree of elastic participation in the acoustic–gravity mode.

6.3. *Energetic meaning of 'elastic leakage'*

The present model is conservative: in the absence of attenuation, energy transferred into the elastic half-space is not lost but becomes part of the coupled fluid–solid mode. In that sense, elasticity does not dissipate triad energy; it redistributes the acoustic-mode energy between the fluid and the solid according to (6.6). If weak attenuation in the solid is included (not considered here), the same partition determines the fraction of triad-fed acoustic energy that is subsequently dissipated in the solid bottom boundary.

In the lossless elastic half-space considered here, the impedance is taken to be real on the branches analysed, so the triad system remains conservative. If attenuation in the solid is included, the effective impedance becomes complex and the modulation equations would acquire genuine decay on the slow time scale.

7. Discussion and conclusions

A central outcome of the present analysis is a clear separation between two distinct roles played by elasticity (and, more generally, compressibility-mediated bottom compliance) in acoustic–gravity wave triad resonance. These roles correspond to two mathematically different regimes of the underlying dispersion problem.

7.1. *Regular regime: perturbative effect when the rigid-bottom triad exists*

When the acoustic–gravity wave member of the triad exists in the rigid-bottom formulation, the corresponding dispersion relation

$$D_r(\omega, \kappa; h) = 0 \tag{7.1}$$

admits a simple real root (ω_0, κ_0), satisfying

$$\frac{\partial D_r}{\partial \omega}(\omega_0, \kappa_0; h) \neq 0. \tag{7.2}$$

In this case, the elastic-bottom dispersion relation derived in the present work may be written in the form

$$D_e(\omega, \kappa; h) = D_r(\omega, \kappa; h) + \mathcal{Z}(\omega, \kappa)Q(\omega, \kappa; h), \tag{7.3}$$

https://doi.org/10.1017/jfm.2026.11735 Published online by Cambridge University Press

where $\mathcal{Z}$ is the effective elastic impedance and Q is given explicitly by (3.10).

By the implicit function theorem, (7.3) admits a unique nearby root

$$\omega_e(\kappa) = \omega_0(\kappa) + O(\mathcal{Z}), \tag{7.4}$$

and hence the elastic correction to the acoustic–gravity wave frequency is perturbatively small. Using the dispersion-derivative identity (5.25) established in § 5.6, the elastic normalisation satisfies

$$\mathcal{N}_e = \frac{1}{2\omega}\frac{\partial D_e}{\partial \omega} = \mathcal{N}_r\big(1 + O(\mathcal{Z})\big), \tag{7.5}$$

where $\mathcal{N}_r = (2\omega)^{-1}\partial_\omega D_r$ is the rigid-bottom normalisation.

Since the quadratic forcing responsible for the triad interaction arises solely from free-surface nonlinearities, the coupling coefficient in the elastic case retains the form

$$\delta_e = \frac{\mathcal{P}}{\mathcal{N}_e}, \tag{7.6}$$

where $\mathcal{P}$ is the same quadratic projection coefficient as in the rigid-bottom theory and is therefore independent of the bottom model at the order considered. Denoting by

$$\delta_r = \frac{\mathcal{P}}{\mathcal{N}_r} \tag{7.7}$$

the corresponding rigid-bottom coupling coefficient, we obtain

$$\frac{\delta_e}{\delta_r} = \frac{\mathcal{N}_r}{\mathcal{N}_e} = 1 + O(\mathcal{Z}). \tag{7.8}$$

Hence, when the rigid-bottom triad already exists, elasticity produces only a perturbatively small correction to the coupling strength, and therefore to the associated growth rate and slow modulation dynamics. In this regular regime, elasticity acts as a weak correction to the classical rigid-bottom theory.

7.2. *Singular regime: elasticity as a mechanism for admitting triad resonance*

A fundamentally different situation arises near the rigid-bottom cutoff. In shallow configurations, the rigid-bottom dispersion relation ceases to admit a propagating acoustic–gravity wave solution; mathematically, this corresponds to a degeneracy characterised by

$$D_r(\omega_c, \kappa_c; h_c) = 0, \qquad \frac{\partial D_r}{\partial \omega}(\omega_c, \kappa_c; h_c) = 0. \tag{7.9}$$

At such points, the rigid-bottom acoustic–gravity wave branch terminates and no triad closure is possible.

Near the cutoff, the rigid dispersion relation has a non-degenerate turning-point expansion

$$D_r \approx \frac{1}{2} D_{\omega\omega}(\omega_c, \kappa_c; h_c)(\omega - \omega_c)^2 + D_h(\omega_c, \kappa_c; h_c)(h - h_c), \tag{7.10}$$

with $D_{\omega\omega}(\omega_c, \kappa_c; h_c) \neq 0$ at this first cutoff. The cutoff-shift argument below depends only on this non-degeneracy, not on the sign of $D_{\omega\omega}$. Since the elastic contribution enters additively through $\mathcal{Z}Q$, the perturbed cutoff is obtained by setting $D_e = 0$, which yields the leading-order shift

$$h_c^{(e)} - h_c^{(r)} \approx -\frac{\mathcal{Z}(\omega_c, \kappa_c)\, Q(\omega_c, \kappa_c; h_c)}{D_h(\omega_c, \kappa_c; h_c)}. \tag{7.11}$$

https://doi.org/10.1017/jfm.2026.11735 Published online by Cambridge University Press

For the first rigid cutoff (with $\kappa \simeq 0$), one has $\alpha h = \pi/2$, so $\cos(\alpha h) = 0$ and $\sin(\alpha h) = 1$. At this point

$$Q(\omega_c, \kappa_c; h_c) = -\frac{\omega_c^2}{\alpha_c} < 0, \qquad D_h(\omega_c, \kappa_c; h_c) = \partial_h D_r = \omega_c^2 \alpha_c > 0, \tag{7.12}$$

so $Q/D_h < 0$. For the conservative weak-coupling branch considered here, Appendix A shows that $\mathcal{Z}(\omega_c, \kappa_c) < 0$. Hence, $\mathcal{Z}\, Q > 0$ and (7.11) gives $h_c^{(e)} - h_c^{(r)} < 0$: elastic coupling reduces the cutoff depth, consistent with the physical picture that a compliant interface restores a guided acoustic–gravity mode in shallower configurations.

Thus, even weak elastic coupling can restore a propagating acoustic–gravity wave mode in depth regimes where the rigid-bottom theory predicts evanescence. In this singular regime, elasticity does not merely perturb an existing triad; it alters the very admissibility of the acoustic member and thereby enables triad resonance. This distinction is reflected directly in the solvability condition derived in the present work. The elastic interface contribution to the normalisation

$$\mathcal{N}_{int} = 2\omega \frac{\partial \mathcal{Z}}{\partial \omega} |\Phi_e(-h)|^2, \tag{7.13}$$

vanishes in the rigid limit but becomes dynamically significant precisely when the rigid-bottom normalisation degenerates near cutoff. Physically, this term represents the exchange of energy between the fluid and the compliant seabed (or more generally bottom boundary), which becomes decisive when the acoustic mode is marginally trapped.

7.3. *Experimental feasibility and laboratory-scale realisation*

The removal of the rigid-bottom cutoff by elastic coupling has a direct experimental implication: resonant triads can be realised at significantly smaller depths and frequencies than required over a rigid bed. For example, in a laboratory tank with $h \sim 0.2$–0.5 m one can generate nearly counter-propagating gravity wavetrains with $k \sim 6$–$10\,\mathrm{m}^{-1}$ (wavelengths $\lambda \sim 0.6$–1.0 m) and frequencies $f \sim 1$–2 Hz, so that the triad acoustic–gravity frequency is $f \sim 2$–4 Hz. Under rigid-bottom conditions the corresponding acoustic–gravity mode may be evanescent in such shallow configurations, whereas a compliant substrate (approximating an elastic half-space) can support an interface-guided acoustic–gravity branch that remains admissible. This increases the feasibility of controlled laboratory measurements of triad-driven energy exchange, including direct interrogation of the coupling and detuning coefficients through envelope dynamics. However, practical realisation of the nonlinear triad resonance in laboratory conditions is not guaranteed.

7.4. *Practical feasibility maps*

Admissibility of an elastic acoustic–gravity branch is a necessary condition for triad resonance, but it does not by itself indicate whether the resulting acoustic signal is measurable in a finite facility. In the present paper, all feasibility calculations are restricted to the conservative guided branches described in Appendix A; radiating or leaky branches are excluded from the weakly nonlinear framework adopted here. To connect the theory to observability, we introduce the detection margin $\mathcal{M} \equiv p_{cap}/p_{detect}$, where p_{cap} is the acoustic pressure predicted to be reached within the available interaction time and p_{detect} is a nominal detection threshold. For each candidate configuration, the acoustic member of the triad is obtained from the full elastic dispersion relation (3.7), and its modal normalisation is evaluated using the dispersion-derivative identity (5.25). The operating

https://doi.org/10.1017/jfm.2026.11735 Published online by Cambridge University Press

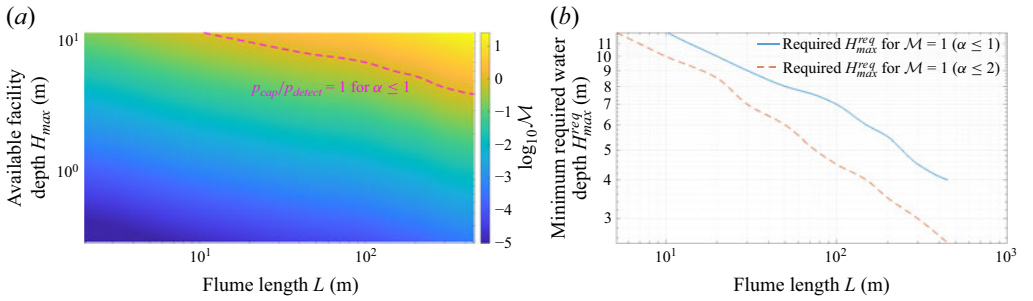


Figure 2. Generic facility-scale feasibility for observing acoustic–gravity triad resonance. (*a*) Detection margin $\log_{10}\mathcal{M}$ in the $(L,\ H^{req}_{max})$ plane, after optimisation over admissible operating conditions and realistic Newtonian fluid–solid pairs; the dashed contour marks $\mathcal{M} = 1$ for the stricter cap $\alpha \leqslant 1$. (*b*) Minimum required depth H^{req}_{max} versus flume length L for two weak-nonlinearity caps, $\alpha \leqslant 1$ and $\alpha \leqslant 2$.

point is then optimised over admissible depths $h \leqslant H^{req}_{max}$ and acoustic frequencies below a prescribed gravity–capillary safety limit, while enforcing a weakly nonlinear validity cap on the forcing amplitude. The available interaction time is taken as the smaller of the viscous damping time and the flume transit time.

Optimisation over realistic fluid–solid pairs shows that detectability improves strongly with both flume length L and maximum usable depth H^{req}_{max} (see figure 2), with depth emerging as the dominant control parameter over the range examined, i.e. shallow facilities remain well below threshold across the range of L, whereas sufficiently deep facilities become plausible even at moderate lengths (figure 2*a*). Relaxing the weak-nonlinearity cap (from $\alpha \leqslant 1$ to $\alpha \leqslant 2$) reduces the minimum depth needed for $\mathcal{M} \gtrsim 1$ (figure 2*b*), but does not change the basic conclusion that depth is the primary control parameter, with L entering mainly through the available interaction time.

Since small/medium flumes seem to be practically unfavourable for the sought triad-resonance experiment, we next focus attention on large water flumes (with water as the working fluid), varying only the substrate within the material catalogue considered here; the facility dimensions used as constraints are listed in table 1. Under the stricter cap $\alpha \leqslant 1$, the deepest facilities provide the best prospects, while more limited depths remain below threshold even with favourable substrates (figure 3*a*). Increasing α_{max} can move marginal cases toward detectability, but it does not eliminate the strong ordering with facility depth (figure 3*b*). Thus, although elasticity removes the rigid-bottom cutoff and enlarges the admissible triad parameter space, the more stringent practical conclusion is that an observable signal in water still requires very large and, especially, deep facilities; variations in substrate properties provide only secondary improvement compared with increasing usable depth.

7.5. *Outlook*

Several directions for future work emerge naturally from the present study. A systematic evaluation of the elastic impedance for realistic bottom boundary materials would enable mapping of admissible triads and coefficient variations across parameter space. Incorporating weak attenuation in the solid would quantify how elastic participation, measured by $\mathcal{N}_{int}/\mathcal{N}_e$, translates into measurable decay of acoustic energy in long-time dynamics. It is worth noting that the analysis presented here follows the triad setting of Kadri & Akylas (2016); in regimes where the acoustic horizontal length scale is much larger than the water depth, a different asymptotic ordering applies and the corresponding

https://doi.org/10.1017/jfm.2026.11735 Published online by Cambridge University Press

Facility	Location	L [m]	W [m]	H_{max}^{req} [m]
TIWTE large wave flume	Tianjin, China	456	5.0	12.0
Delta flume (Deltares)	Netherlands	300	5.0	9.5
Large wave flume / GWK	Hannover, Germany	300	5.0	7.0
Large hydro-geo flume (PARI)	Japan	184	3.5	12.0
O.H. Hinsdale large wave flume	Oregon State, USA	104	3.7	2.7
CIEM large-scale wave flume	UPC, Spain	100	3.0	4.5

Table 1. Large experimental water flumes considered in the water-only facility analysis. Here, L is the flume length, W is the quoted width and H_{max}^{req} is the maximum stated operating water depth used as the upper depth constraint in the feasibility calculations.

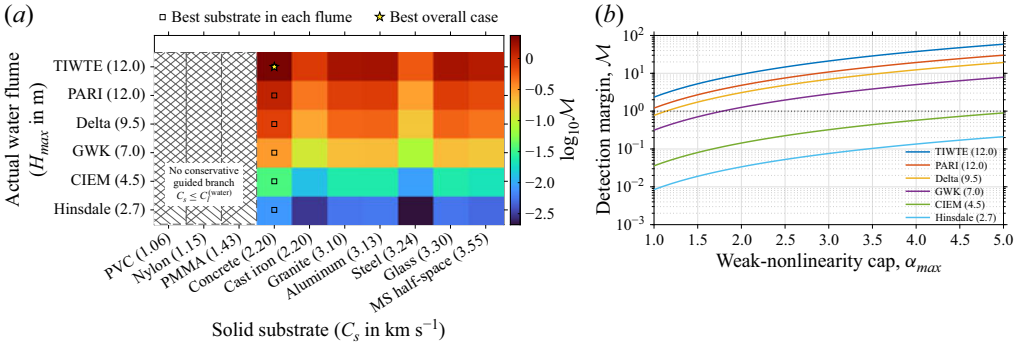


Figure 3. Water-only feasibility in selected large flumes, computed as in § 7.4. (*a*) Detection margin $\log_{10}\mathcal{M}$ for each flume–substrate pair under the stricter cap $\alpha \leqslant 1$; open squares indicate the best substrate within each flume and the star denotes the overall best case. Hatched columns indicate substrates for which no conservative guided branch exists in the present model ($C_s \leqslant c$, so the interval $\omega/C_s < \kappa < \omega/c$ is empty). (*b*) Optimised detection margin versus α_{max} for each flume, maximised over admissible $(h,\ f)$ and over the valid substrate set.

evolution equations would need to be re-derived. Finally, extension to acoustic–gravity-capillary triad resonance, three-dimensional geometries, and layered or poroelastic bottom structures would broaden applicability to laboratory experiments, coastal acoustics and geophysical settings.

Acknowledgements. This work was supported by the Leverhulme Trust Research Project Grant number 523930. AI tools were used for language editing; and all scientific content, analysis, and conclusions are the author's own.

Declaration of interests. The author reports no conflict of interest.

Data availability statement. The data that support the findings of this study are available from the corresponding author upon reasonable request.

Appendix A. Elastic half-space impedance and dispersion relation

For completeness, we present the effective impedance condition at the fluid–elastic solid interface for a homogeneous isotropic elastic half-space and the resulting finite-depth acoustic–gravity dispersion relation. The detailed elimination of the elastic potentials is given in Eyov *et al.* (2013); here we present the final expressions in the notation of the present paper.

https://doi.org/10.1017/jfm.2026.11735 Published online by Cambridge University Press

A.1. *Governing equations in the solid*

In the elastic half-space $z \leqslant -h$, the displacement $\boldsymbol{u}_s = (u_s, w_s)$ satisfies linear elasticity

$$\rho_s \boldsymbol{u}_{s,tt} = (\lambda_s + \mu_s)\boldsymbol{\nabla}(\boldsymbol{\nabla} \cdot \boldsymbol{u}_s) + \mu_s \boldsymbol{\nabla}^2 \boldsymbol{u}_s, \tag{A1}$$

where ρ_s is the solid density and (λ_s, μ_s) are Lamé parameters. Introducing scalar and vector potentials ϕ_s and $\boldsymbol{\psi}_s = (0, \psi_s, 0)$

$$\boldsymbol{u}_s = \boldsymbol{\nabla}\phi_s + \boldsymbol{\nabla} \times \boldsymbol{\psi}_s, \tag{A2}$$

the potentials satisfy

$$\boldsymbol{\nabla}^2 \phi_s = \frac{1}{C_p^2}\phi_{s,tt}, \qquad \boldsymbol{\nabla}^2 \psi_s = \frac{1}{C_s^2}\psi_{s,tt}, \tag{A3}$$

with compressional and shear speeds $C_p = \sqrt{(\lambda_s + 2\mu_s)/\rho_s}$ and $C_s = \sqrt{\mu_s/\rho_s}$.

A.1. *Spectral variables*

We consider two-dimensional time-harmonic dependence $\exp\{\mathrm{i}(\kappa x - \omega t)\}$. In the fluid

$$\Phi_{zz} + \alpha^2 \Phi = 0, \qquad \alpha^2 = \frac{\omega^2}{c^2} - \kappa^2, \qquad -h \leqslant z \leqslant 0, \tag{A4}$$

and the linear free-surface condition is

$$g\Phi_z - \omega^2 \Phi = 0, \qquad z = 0. \tag{A5}$$

We take the branch $\alpha = \sqrt{\omega^2/c^2 - \kappa^2}$ with $\Re(\alpha) \geqslant 0$.

In the elastic half-space, decay as $z \to -\infty$ introduces the vertical wavenumbers

$$q_p = \sqrt{\kappa^2 - \frac{\omega^2}{C_p^2}}, \qquad q_s = \sqrt{\kappa^2 - \frac{\omega^2}{C_s^2}}, \tag{A6}$$

with square-root branches chosen such that $\Re(q_p) > 0$ and $\Re(q_s) > 0$ (so that the elastic fields decay as $z \to -\infty$). In the present lossless setting we focus on real ω and κ on conservative (non-radiating) branches of the coupled dispersion relation. Depending on (ω, κ), q_p and/or q_s may be complex; this corresponds to radiating/leaky behaviour in the half-space and is not pursued here, since the weakly nonlinear triad reduction is formulated for the conservative (Hamiltonian) regime.

A.3. *Exact impedance boundary condition at $z = -h$*

Imposing continuity of vertical velocity and normal traction, together with vanishing shear traction at the interface (liquid cannot support shear), the elastic variables may be eliminated to give an effective impedance condition on the fluid potential

$$\phi_{l,z} - \mathcal{Z}(\omega, \kappa)\phi_l = 0, \qquad z = -h. \tag{A7}$$

The exact half-space impedance may be written as

$$\mathcal{Z}(\omega, \kappa) = \underbrace{\frac{\rho_l \omega^2}{\rho_s} \frac{q_p}{\omega^2 - C_s^2 \kappa^2}}_{\mathcal{Z}_{lead}(\omega, \kappa)} \times \underbrace{\mathcal{F}(\omega, \kappa)}_{\text{dimensionless correction}}, \tag{A8}$$

where $\mathcal{Z}_{lead}$ gives the leading impedance scaling obtained by eliminating the elastic potentials (up to the sign convention implied by $\exp\{\mathrm{i}(\kappa x - \omega t)\}$ and the definition of

https://doi.org/10.1017/jfm.2026.11735 Published online by Cambridge University Press

normal traction), and $\mathcal{F}$ is a dimensionless correction accounting for shear coupling and mode conversion in the half-space

$$\mathcal{F}(\omega,\kappa)=\frac{1}{1+4\kappa^2 q_p q_s\left(\omega^2/C_s^2-2\kappa^2\right)^{-2}}\frac{\kappa^2+q_s^2}{\kappa^2-q_s^2}. \tag{A9}$$

In the conservative guided regime considered here (real ω, κ with decaying elastic fields), the effective impedance is real. With the present sign convention, $\mathcal{Z}_{lead}$ is negative when q_p is real and $\kappa^2>\omega^2/C_s^2$; in the weak-coupling guided branches examined in this paper, the full impedance $\mathcal{Z}$ has the same sign.

Using $\kappa^2-q_s^2=\omega^2/C_s^2$ allows $\mathcal{Z}$ to be written explicitly as

$$\mathcal{Z}(\omega,\kappa)=-\frac{\rho_l}{\rho_s}\frac{q_p\,(\kappa^2+q_s^2)}{\kappa^2-\omega^2/C_s^2}\left[1+4\kappa^2 q_p q_s\left(\omega^2/C_s^2-2\kappa^2\right)^{-2}\right]^{-1}. \tag{A10}$$

Equivalently, since $\kappa^2+q_s^2=2\kappa^2-\omega^2/C_s^2$, (A10) may be written entirely in terms of (ω,κ) as

$$\mathcal{Z}(\omega,\kappa)=-\frac{\rho_l}{\rho_s}\frac{\sqrt{\kappa^2-\dfrac{\omega^2}{C_p^2}}\left(2\kappa^2-\dfrac{\omega^2}{C_s^2}\right)}{\kappa^2-\dfrac{\omega^2}{C_s^2}}\left[1+\frac{4\kappa^2\sqrt{\kappa^2-\dfrac{\omega^2}{C_p^2}}\sqrt{\kappa^2-\dfrac{\omega^2}{C_s^2}}}{\left(\dfrac{\omega^2}{C_s^2}-2\kappa^2\right)^2}\right]^{-1}. \tag{A11}$$

Equations (A7)–(A11) are algebraically equivalent to the half-space reduction in Eyov *et al.* (2013), rewritten in the present notation.

A.4. *Finite-depth dispersion relation*

Combining the fluid eigenproblem, the free-surface condition, and the impedance boundary condition yields the dispersion relation used in the main text

$$\begin{aligned}D_e(\omega,\kappa;h)\equiv{}& g\big[-\alpha\sin(\alpha h)+\mathcal{Z}(\omega,\kappa)\cos(\alpha h)\big]-\omega^2\left[\cos(\alpha h)+\frac{\mathcal{Z}(\omega,\kappa)}{\alpha}\sin(\alpha h)\right]\\ ={}&0.\end{aligned} \tag{A12}$$

Appendix B. Recovery of the rigid-bottom resonant-triad framework

For completeness, we show explicitly how the present formulation reduces to the classical rigid-bottom acoustic–gravity resonant-triad framework in the appropriate limit. In the rigid-bottom case, the interface condition reduces to

$$\phi_{l,z}=0,\qquad z=-h. \tag{B1}$$

With the impedance convention (2.9), this corresponds to the limit $\mathcal{Z}\to 0$. The boundary operator $\mathcal{B}_e$ is independent of spectral parameters, and hence

$$\partial_\omega\mathcal{B}_e=\partial_\kappa\mathcal{B}_e=0. \tag{B2}$$

As a result, the interface contribution $\mathcal{I}_e$ in the solvability condition vanishes identically. The acoustic-mode normalisation reduces to the classical free-surface contribution

$$\mathcal{N}_e\to\mathcal{N}_{fs}, \tag{B3}$$

https://doi.org/10.1017/jfm.2026.11735 Published online by Cambridge University Press

and the coupling and detuning coefficients recover their rigid-bottom forms. The triad evolution equations and their associated invariants coincide with those obtained in previous rigid-bottom analyses.

Appendix C. Large experimental water flumes used in the feasibility analysis

For the feasibility analysis in § 7.4, we considered a set of large hydraulic and coastal research flumes whose publicly stated lengths and maximum water depths are sufficiently well documented to define practical facility constraints. In each case, the flume length L was used in the transit-time estimate, while the maximum usable water depth H_{max}^{req} was used as the upper bound in the depth optimisation. The quoted widths are included for context only and were not used explicitly in the present one-dimensional observability proxy. Because public descriptions of these facilities are not perfectly uniform, the values in table 1 should be interpreted as practical working dimensions rather than as a strict ranking by geometric volume.

References

ACHENBACH, J.D. 1973 *Wave Propagation in Elastic Solids*. North-Holland.

ANDRADE, J.S., BUSTAMANTE, M., KADRI, U. & STUHLMEIER, R. 2025 Phase-space structure of resonant wave triads. *J. Fluid Mech.* **1013**, A23.

ARDHUIN, F. & HERBERS, T.H.C. 2013 Noise generation in the solid Earth, oceans and atmosphere, from nonlinear interacting surface gravity waves in finite depth. *J. Fluid Mech.* **716**, 316–348.

BIOT, M.A. 1952 The interaction of Rayleigh and Stoneley waves in the ocean bottom. *Bull. Seismol. Soc. Am.* **42** (1), 81–93.

BRETHERTON, F.P. 1964 Resonant interactions between waves. The case of discrete oscillations. *J. Fluid Mech.* **20**, 457–479.

CRAIK, A.D.D. 1985 *Wave Interactions and Fluid Flows*. Cambridge University Press.

DALRYMPLE, R.A. & ROGERS, B.D. 2006 A note on wave celerities on a compressible fluid. In *Coastal Engineering 2006: Proceedings of the 30th International Conference on Coastal Engineering* (ed. J. McKee Smith), pp. 3–13. World Scientific.

EYOV, E., KLAR, A., KADRI, U. & STIASSNIE, M. 2013 Progressive waves in a compressible-ocean with an elastic bottom. *Wave Motion* **50** (5), 929–939.

HASSELMANN, K. 1963 A statistical analysis of the generation of microseisms. *Rev. Geophys.* **1** (2), 177–210.

KADRI, U. & AKYLAS, T.R. 2016 On resonant triad interactions involving surface gravity waves and acoustic–gravity waves. *J. Fluid Mech.* **788**, 412–442.

KADRI, U. & STIASSNIE, M. 2013 Acoustic–gravity waves interacting with surface gravity waves. *J. Fluid Mech.* **735**, R6.

LONGUET-HIGGINS, M.S. 1950 A theory of the origin of microseisms. *Phil. Trans. R. Soc. A* **243**, 1–35.

PHILLIPS, O.M. 1960 On the dynamics of unsteady gravity waves of finite amplitude. *J. Fluid Mech.* **9**, 193–217.

PHILLIPS, O.M. 1981 Wave interactions – the evolution of an idea. *J. Fluid Mech.* **106**, 215–227.

STIASSNIE, M. 2010 Tsunamis and acoustic-gravity waves from underwater earthquakes. *J. Engng Maths* **67**, 23–32.

https://doi.org/10.1017/jfm.2026.11735 Published online by Cambridge University Press